Supporting information

# $CO_2$-assisted synthesis of crystalline/amorphous NiFe-MOF heterostructure for high-efficiency electrocatalytic water oxidation

Yifan Li,[a] Wenjie Ma,*[b] Huanhuan Yang,[b] Qingyong Tian,[b] Qun Xu,*[a,b] Buxing Han*[c]

College of Materials Science and Engineering, Zhengzhou University, Zhengzhou 450052, P. R. China. E-mail: qunxu@zzu.edu.cn

**Content**

**Experimental section**

**Materials.** Nickel (II) chloride hexahydrate ($NiCl_2 \cdot 6H_2O$, 99.0%), Iron (II) chloride tetrahydrate ($FeCl_2 \cdot 4H_2O$, 99.0%), 1,4-Benzenedicarboxylic acid (1,4-BDC, AR grade), N, N-dimethylformamide (DMF, AR grade), ethanol (AR grade) and Sodium hydroxide (NaOH, AR grade) are purchased from Sinopharm Chemical Reagent Co. Ltd. Triethylamine (TEA) and Potassium hydroxide (KOH, 95%, AR grade) are purchased from Aladdin. Nafion solution (5 wt.%) is purchased from Sigma-Aldrich. Nickel (II) nitrate hexahydrate [Ni $(NO_3)_2 \cdot 6H_2O$, AR grade] is purchased from Jiangsu Qiangsheng Functional Chemistry Co., Ltd and Ferric chloride hexahydrate ($FeCl_3 \cdot 6H_2O$, AR grade) is purchased from Shanghai Forneeds Biological Technology Co., Ltd.

**Synthesis of *c/a*-NiFe-MOF:** For the synthesis of *c/a*-NiFe-MOF using $CO_2$-assisted technology, 10 mL of N, N-dimethylformamide (DMF), 0.67 mL of ethanol and 0.67 mL of deionized water are first added into a 30 mL glass bottle. Then, 0.25 mmol of 1, 4-benzenedicarboxylic acid (1, 4-BDC) is ultrasonically dispersed in above solution. Next, 0.1875 mmol of $NiCl_2 \cdot 6H_2O$ and 0.0625 mmol of $FeCl_2 \cdot 4H_2O$ are added. After stirring for 5 min, 0.33 mL of triethylamine (TEA) is injected into the solution quickly to form the homogeneous colloidal suspensions, and the solution is added into autoclave. Then $CO_2$ is charged into the autoclave under stirring to the desired pressure of 7.5 MPa for 3 h at 35 °C. The resulting product is washed with ethanol and DMF, then the product was dried at 60 °C in vacuum for 12 h.

**Synthesis of Ni-MOF:** For the synthesis of Ni-MOF using $CO_2$-assisted technology, 10 mL of DMF, 0.67 mL of ethanol and 0.67 mL of deionized water are first added into a 30 mL glass bottle. Then, 0.25 mmol of 1, 4-BDC is ultrasonically dispersed in above solution. Next, 0.25 mmol of $NiCl_2 \cdot 6H_2O$ is added. After stirring for 5 min, 0.33 mL of TEA is injected into the solution quickly to form the homogeneous colloidal suspensions, and the solution is added into autoclave. Then $CO_2$ is charged into the autoclave under stirring to the desired pressure of 7.5 MPa for 3 h at 35 °C. The resulting product is washed with ethanol and DMF, then the product was dried at 60 °C in vacuum for 12 h.

**Synthesis of Fe-MOF:** For the synthesis of Fe-MOF using $CO_2$-assisted technology,

10 mL of DMF, 0.67 mL of ethanol and 0.67 mL of deionized water are first added into a 30 mL glass bottle. Then, 0.25 mmol of 1, 4-BDC is ultrasonically dispersed in above solution. Next, 0.25 mmol of $FeCl_2 \cdot 4H_2O$ is added. After stirring for 5 min, 0.33 mL of TEA is injected into the solution quickly to form the homogeneous colloidal suspensions, and the solution is added into autoclave. Then $CO_2$ is charged into the autoclave under stirring to the desired pressure of 7.5 MPa for 6 h at 35 °C. The resulting product is washed with ethanol and DMF, then the product was dried at 60 °C in vacuum for 12 h.

**Synthesis of Amorphous NiFe-BDC (*a*-NiFe-BDC):** For the synthesis of *a*-NiFe-BDC using $CO_2$-assisted technology, 10 mL of DMF, 0.67 mL of ethanol and 0.67 mL of deionized water are first added into a 30 mL glass bottle. Then, 0.25 mmol of 1, 4-BDC is ultrasonically dispersed in above solution. Next, 0.1875 mmol of $NiCl_2 \cdot 6H_2O$ and 0.0625 mmol of $FeCl_2 \cdot 4H_2O$ are added. After stirring for 5 min, 0.33 mL of TEA is injected into the solution quickly to form the homogeneous colloidal suspensions, and the solution is added into autoclave. Then $CO_2$ is charged into the autoclave under stirring to the desired pressure of 7.5 MPa for 1 h at 35 °C. The resulting product is washed with ethanol and DMF, then the product was dried at 60 °C in vacuum for 12 h.

**Synthesis of FeNi-MIL-88B:** For the synthesis of FeNi-MIL-88B, 30 mL of DMF is added into a 100 mL beaker. Then, 2.8 mmol of 1, 4-BDC, 1.2 mmol of Ni $(NO_3)_2 \cdot 6H_2O$ and 1.6 mmol of $FeCl_3 \cdot 6H_2O$ are added. After stirring for 15 min, 3 ml of 0.4 M NaOH solution is added. Finally, the mixed solution is transferred to a 50 mL reaction kettle at 130 °C for 12 h.

**Synthesis of Mixed catalyst:** For the synthesis of Mixed catalyst, 15 mg of FeNi-MIL-88B and 15 mg of amorphous NiFe-BDC are added into a mortar and grinding for 10 min. Finally, we get mixed catalyst powder.

**Synthesis of $CO_2$-free NiFe-MOF:** For the synthesis of $CO_2$-free NiFe-MOF, 10 mL of DMF, 0.67 mL of ethanol and 0.67 mL of deionized water are first added into a 30 mL glass bottle. Then, 0.25 mmol of 1, 4-BDC is ultrasonically dispersed in above solution. Next, 0.1875 mmol of $NiCl_2 \cdot 6H_2O$ and 0.0625 mmol of $FeCl_2 \cdot 4H_2O$ are

added. After stirring for 5 min, 0.33 mL of TEA is injected into the solution quickly to form the homogeneous colloidal suspensions. The reaction continues under stirring for 3 h at 35 °C, while there is no compressed $CO_2$ is charged into the autoclave in this part of experiment.

**Synthesis of Bulk NiFe-MOF:** For the synthesis of bulk NiFe-BDC, 30 mL of DMF, 2 mL of ethanol and 2 mL of deionized water are added into a 100 mL beaker. Then, 0.75 mmol of 1, 4-BDC is ultrasonically dispersed in the solution. Next, 0.375 mmol of $NiCl_2 \cdot 6H_2O$ and 0.375 mmol of $FeCl_2 \cdot 4H_2O$ are added. Finally, the mixed solution is transferred to a 100 mL reaction kettle at 140 °C for 24 h.

**Synthesis of 2D NiFe-MOF:** For the synthesis of NiFe-MOF nanosheet (2D NiFe-MOF), 30 mL of DMF, 2 mL of ethanol and 2 mL of deionized water are added into a 100 mL beaker. Then, 0.75 mmol of 1, 4-BDC is ultrasonically dispersed in the solution. Next, 0.375 mmol of $NiCl_2 \cdot 6H_2O$ and 0.375 mmol of $FeCl_2 \cdot 4H_2O$ are added. Finally, the mixed solution is the mixed solution is ultrasonically shocked for 8 h.

**Characterization.**

X-ray diffractometer (XRD, Rigaku D/M ax 2550) is applied to confirm the phase structure of all samples. The morphology of the products is studied by transmission electron microscopy (TEM) and scanning transmission electron microscopy (STEM) are acquired by FEI Talos-F200S. Scanning electron microscopy (SEM) images and energy dispersive X-ray spectroscopy (EDS) are taken with a ZEISS Sigma 300 scanning electron microscope operated at 15 kV. X-ray photoelectron spectra (XPS) are collected with an Thermo Scientific K-Alpha$^+$ XPS Spectrometer. FT-IR spectra (KBr pellets) are acquired with a INVENIO R FT-IR spectrometer. Raman spectra are acquired with a INVENIO R FT-IR spectrometer. Raman spectra are recorded at 633 nm excitation wavelength with LabRAMsolell nano.

**Electrochemical measurements.**

Electrochemical tests are performed in alkaline electrolytes (at 1 M KOH concentration). Glassy carbon (GC) disks (geometric area: 0.0704 $cm^2$) are polished with $Al_2O_3$ powders. The ink of the catalyst is made through putting the catalyst (5 mg) into1 mL of mixed solution which is made up of 50 μL of 5 wt% Nafion, 800 μL

of ethanol and 150 μL of deionized water. The obtained catalyst ink is dispersed by ultrasound and 10 μL of the ink is loaded on the surface of the polished GC disk. All electrochemical measurements are carried out using a SP-150 electrochemical workstation with a three-electrode system at room temperature. The working electrode is a glassy carbon electrode (GCE, 3 mm in diameter). The graphite rod and Hg/HgO are used as the counter electrodes and the reference, respectively. The linear sweep voltammograms of the different samples are measured at a scan rate of 5 $mV \cdot s^{-1}$. All measurement results are obtained without iR-compensation. To evaluate the electrochemically active surface areas (ECSA), the double-layer capacitance ($C_{dl}$) is measured via cyclic voltammograms (CV) in the potential range from 0.864 to 0.964 V vs RHE at different scan rates. The electrochemical impedance spectroscopy (EIS) is collected over a scanning frequency from 1 Hz to $10^5$ Hz. The electrode potential versus the saturated calomel electrode is converted to the reversible hydrogen electrode (RHE) potential according to the Nernst equation: E (vs. RHE) = E (vs. HgO) + $E_{HgO}$ + 0.0591 pH).

**Turnover frequency (TOF) calculation.**

The TOF values are calculated via the following equation:

$$TOF = \frac{|j|A}{mFn}$$

where |j| represents the current density at the overpotential of 0.24 V. A is the area of the electrode (0.0704 $cm^2$) and F is the Faradaic constant (96485 $C \cdot mol^{-1}$). m stands for the electrons used to form one $H_2$ or $O_2$ molecule from water (2 electrons for hydrogen evolution reaction and 4 electrons for oxygen evolution reaction). n accounts for the quantity of active sites.

The value of n can be acquired based on ICP results by the following formula:

$$n = \frac{m_{catalyst} \times C_{wt\%-Ni}}{M_{Ni}} + \frac{m_{catalyst} \times C_{wt\%-Fe}}{M_{Fe}}$$

where $m_{catalyst}$ is the catalyst loading on the disk electrode (0.05 mg), $C_{wt\%}$ is the concentration of metal derived from ICP.

The value of n can also be acquired by testing CV at 50 $mV \cdot s^{-1}$ ranging from -0.2 to 0.6 V vs RHE in phosphate buffered saline solution (PBS, pH = 7.0). (The PBS solution is made up of 38 mL of 0.2 M $NaH_2PO_4$ solution and 62 mL of 0.2 M $Na_2HPO_4$. The quantity of active sites is figured out relying on the following formula

(Nano Energy 2018, 51,26–36):

$$n = \frac{Q}{2F} = \frac{i * t}{2F} = \frac{i * V/u}{2F}$$

where Q stands for the cyclic voltammetric capacity acquired by integrating CV cures, F represents the Faradaic constant (96485 $C \cdot mol^{-1}$), i accounts for the current density ($A \cdot m^{-2}$), V is the voltage (v) and u is the scanning rate ($V \cdot s^{-1}$).

## Figures

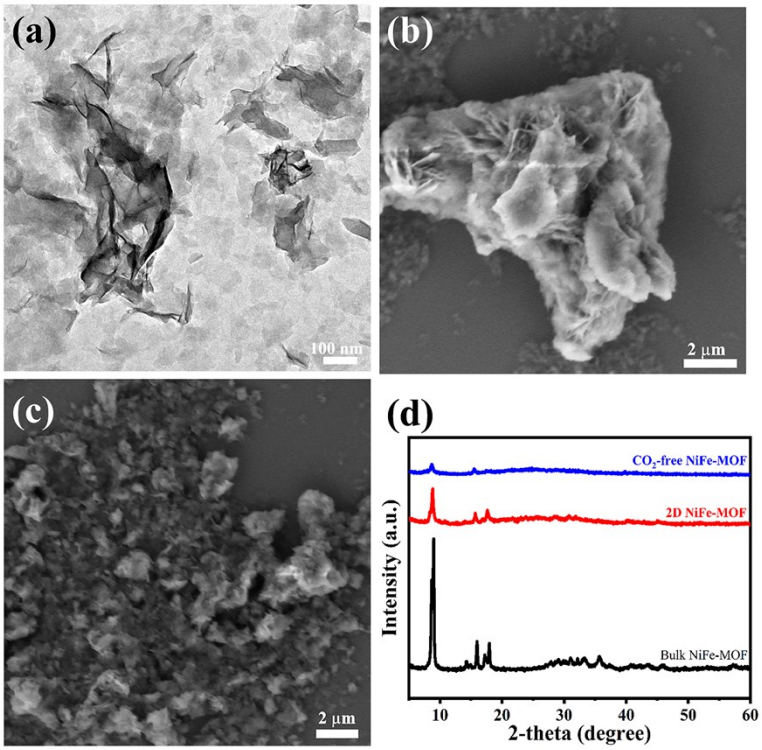


**Fig. S1.** (a) TEM image of 2D NiFe-MOF, (b) SEM image of Bulk NiFe-MOF, (c) SEM image of $CO_2$-free NiFe-MOF, and (d) XRD patterns of 2D NiFe-MOF, Bulk NiFe-MOF and $CO_2$-free NiFe-MOF.

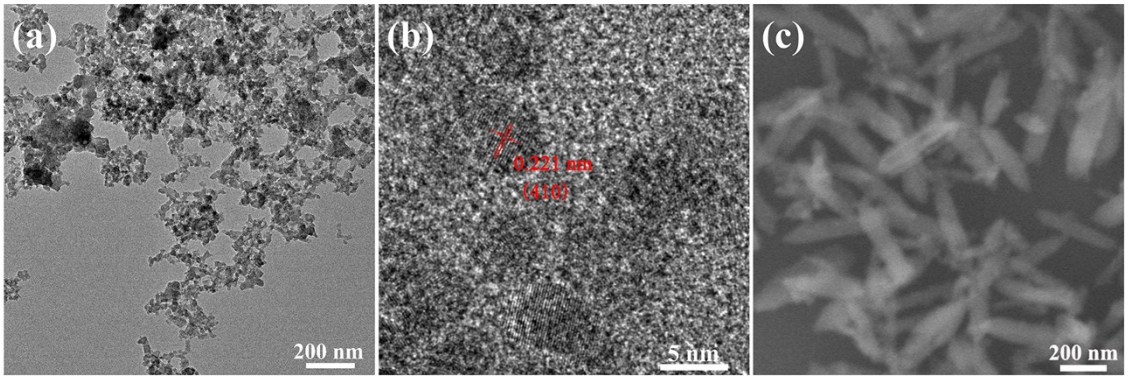


**Fig. S2.** (a-b) TEM and HRTEM images of Ni-MOF, (c) SEM image of Fe-MOF.

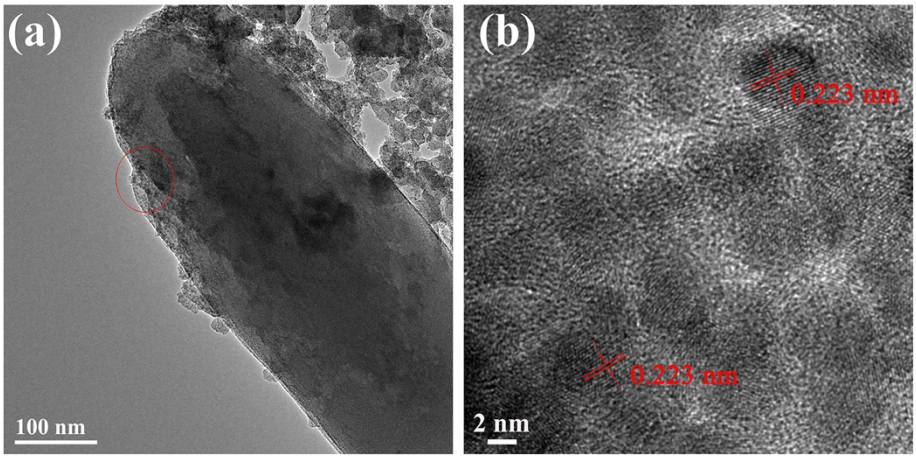


**Fig. S3.** (a-b) The TEM and HRTEM images of the heterostructures.

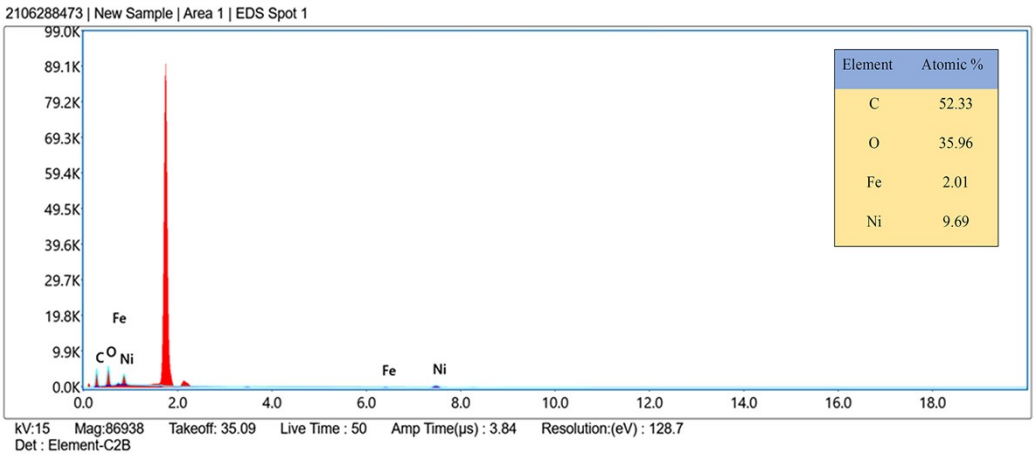


**Fig. S4.** The EDS of nanoparticles in *c/a*-NiFe-MOF.

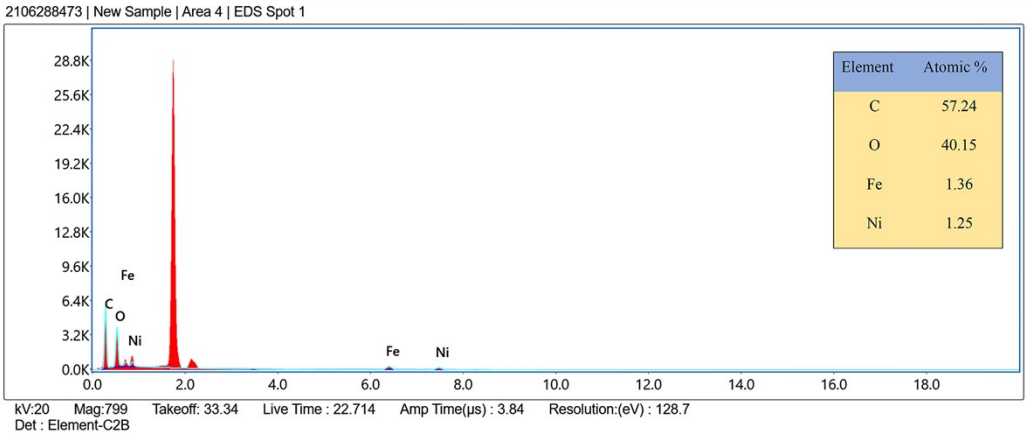


**Fig. S5.** The EDS of the spindles in *c/a*-NiFe-MOF.

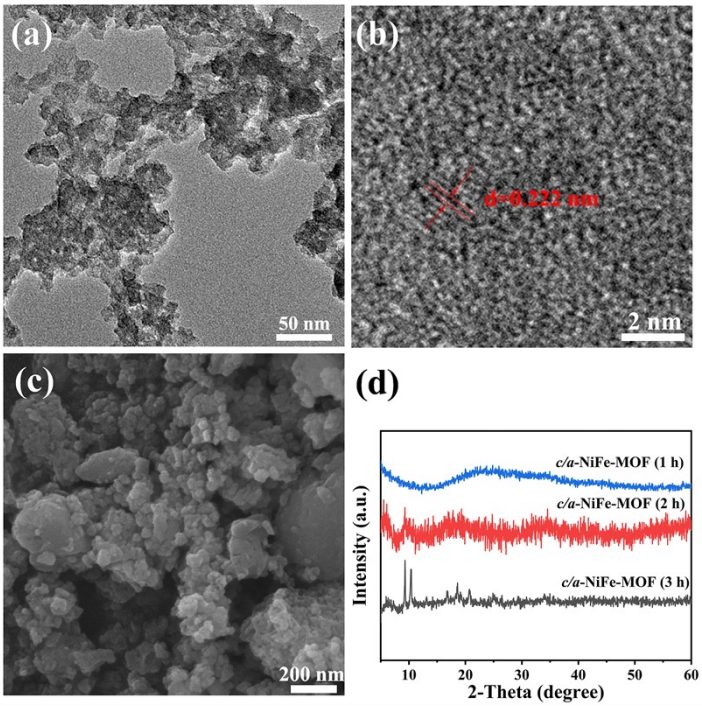


**Fig. S6.** (a-b) TEM and HRTEM images of *c/a*-NiFe-MOF (1 h), (c) SEM image of *c/a*-NiFe-MOF (2 h), and (d) XRD patterns of *c/a*-NiFe-MOF (1 h), *c/a*-NiFe-MOF (2 h) and *c/a*-NiFe-MOF (3 h).

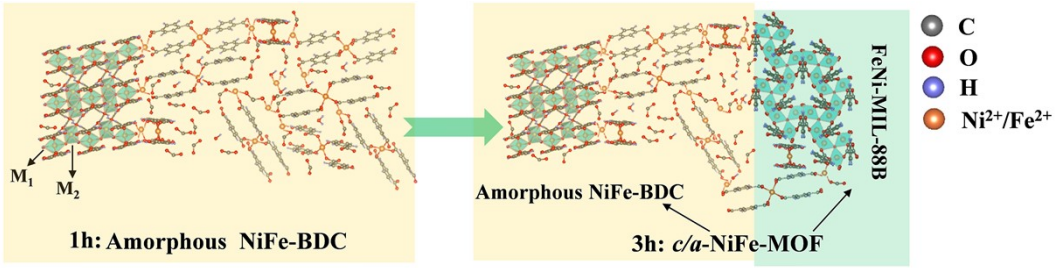


**Fig. S7**. Illustration of phase-transformation process during the synthesis of *c/a*-NiFe-MOF.

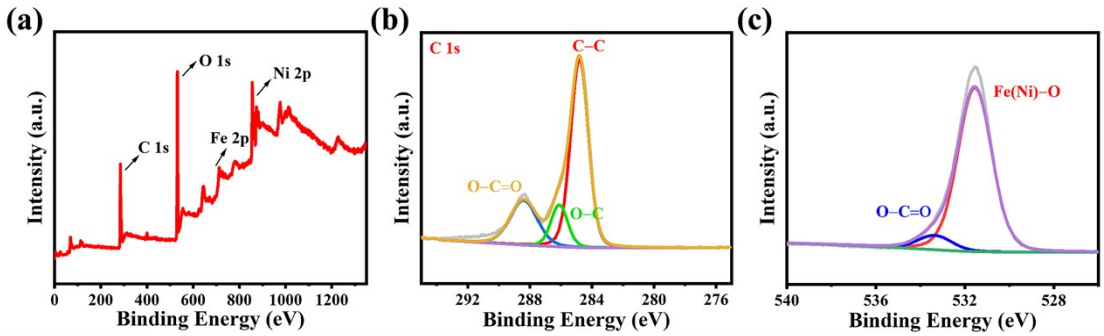


**Fig. S8.** (a) XPS survey spectrum for pristine *c/a*-NiFe-MOF, (b) high resolution XPS spectra of C 1s region: 284.8 eV, 286.1 eV, and 288.4 eV respectively correspond to

the C-C, O-C, and O-C=O bond, (c) high resolution XPS spectra of O 1s region: 531.5 eV and 533.3 eV correspond to the Fe/Ni-O and O-C=O bond.

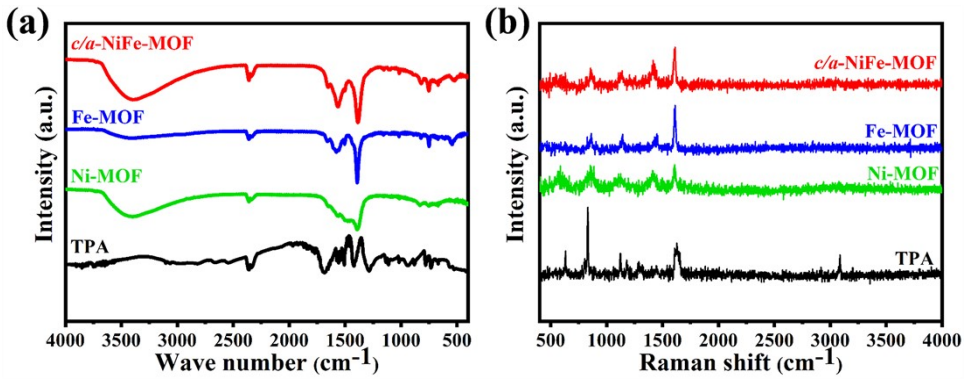


**Fig. S9**. (a) FT-IR spectra of *c/a*-NiFe-MOF, Fe-MOF, Ni-MOF compared with the spectrum of terephthalic acid (TPA) and (b) their corresponding Raman spectra.

In the FT-IR spectra, the peaks at around 3407 $cm^{-1}$ and 748 $cm^{-1}$ of all as-prepared samples correspond to the stretching vibrations of $OH^-$ and the C-H bonding vibrations of the benzene rings.[1] The peaks of ν(Ni/Fe-O) at around 541 $cm^{-1}$ indicate the successful coordination between metal atoms and the organic linker. Furthermore, the peaks at around 1392 $cm^{-1}$ and 1567 $cm^{-1}$ are assigned to the $\nu_s$(-COO-) and $\nu_{as}$(-COO-) originating from coordination bonds between BDC ligands and metal centers.[2] In the Raman spectra, the bands at 1612 $cm^{-1}$ and 1418 $cm^{-1}$ are assigned to the in-plane and out-of-plane stretching modes of the carboxyl group in the samples.[3] The stretching mode C-H groups of benzene ring appear at 852, 813, and 632 $cm^{-1}$.[1, 4]

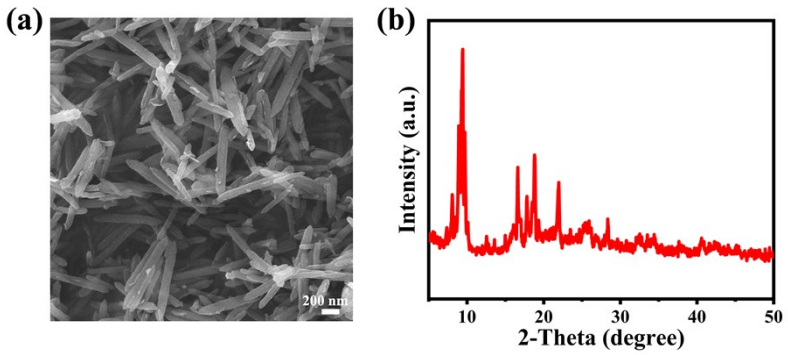


**Fig. S10.** (a) SEM image of FeNi-MIL-88B, (b) XRD pattern of FeNi-MIL-88B.

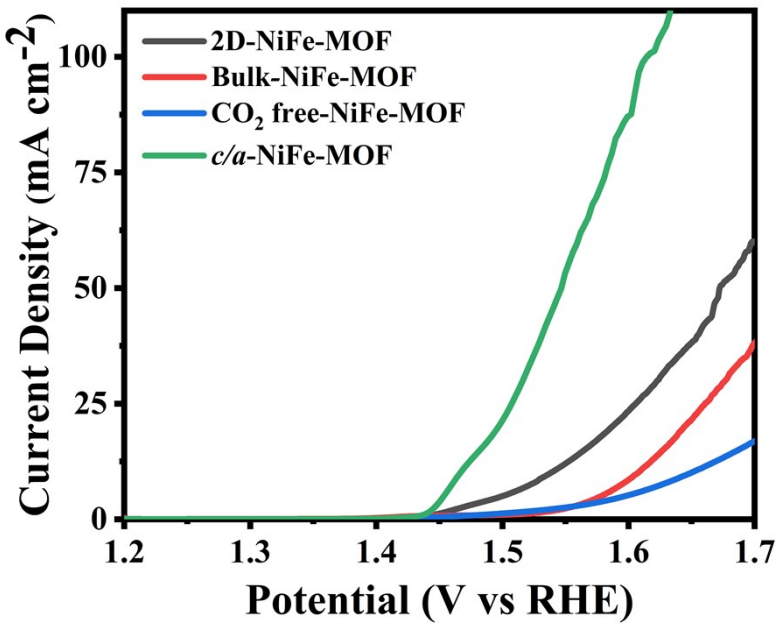


**Fig. S11.** (a) LSV of 2D-NiFe-MOF, Bulk-NiFe-MOF, $CO_2$ free-NiFe-MOF, and *c/a*-NiFe-MOF.

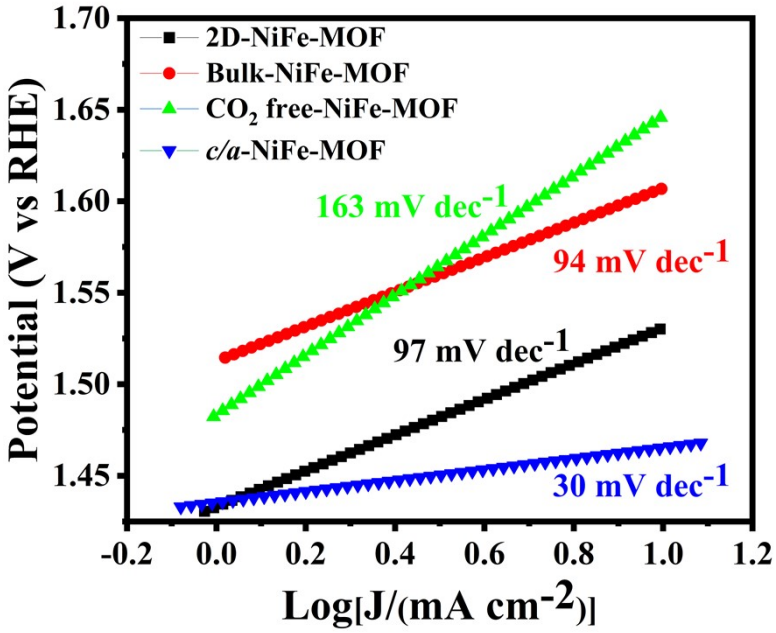


**Fig. S12.** (a) Tafel slopes of 2D-NiFe-MOF, Bulk-NiFe-MOF, $CO_2$ free-NiFe-MOF, and *c/a*-NiFe-MOF.

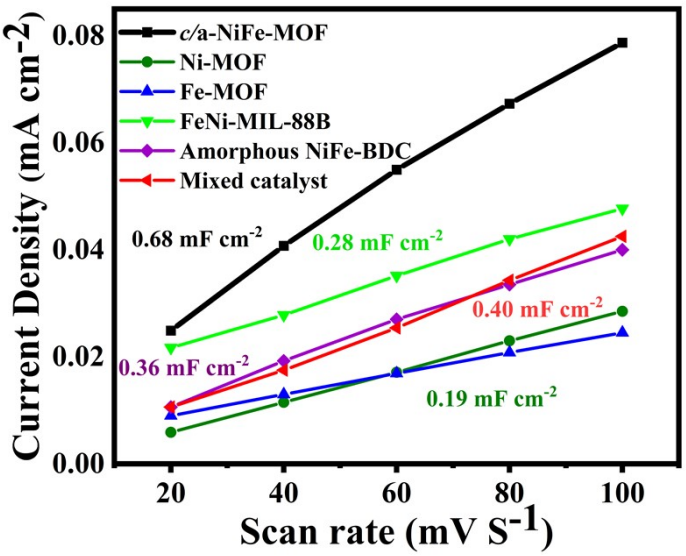


**Fig. S13.** CV current density versus scan rate of different catalysts; the linear slope is equivalent to the double-layer capacitance ($C_{dl}$).

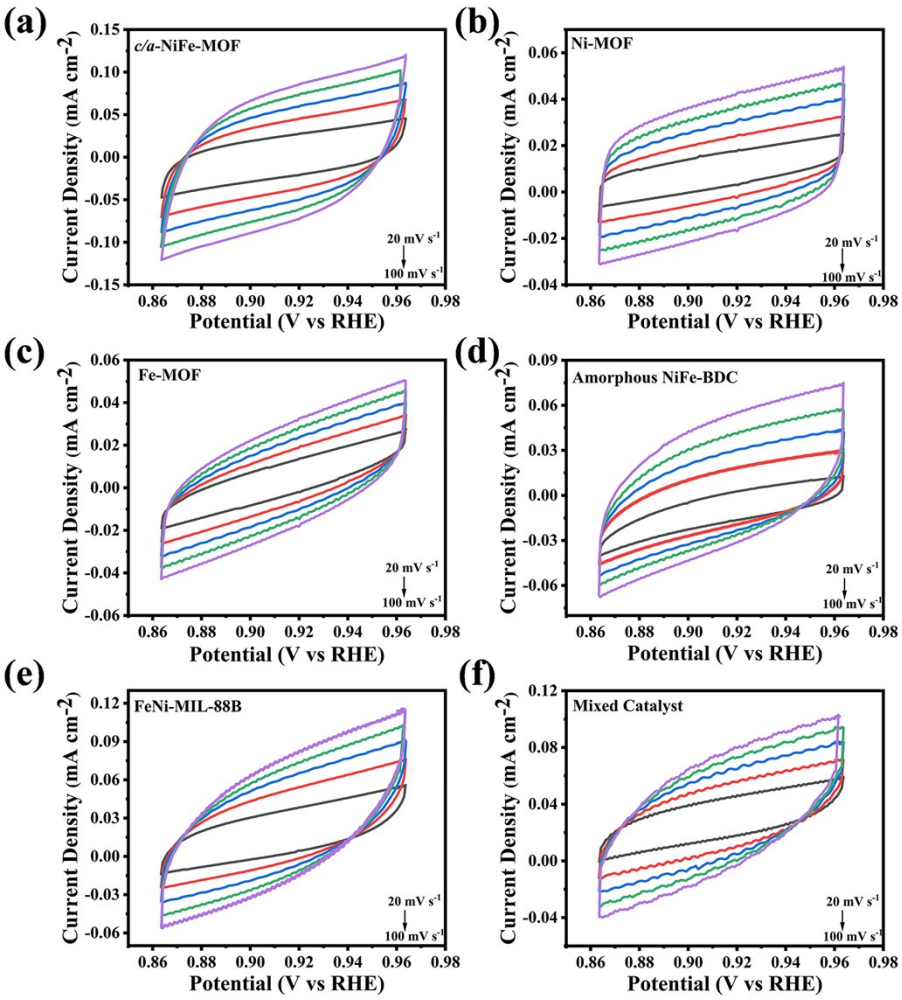


**Fig. S14**. CV curves of (a) *c/a*-NiFe-MOF, (b) Ni-MOF, (c) Fe-MOF, (d) Amorphous NiFe-BDC, (e) FeNi-MIL-88B and (f) Mixed Catalyst at different scan rates from 20

to 100 mV $s^{-1}$.

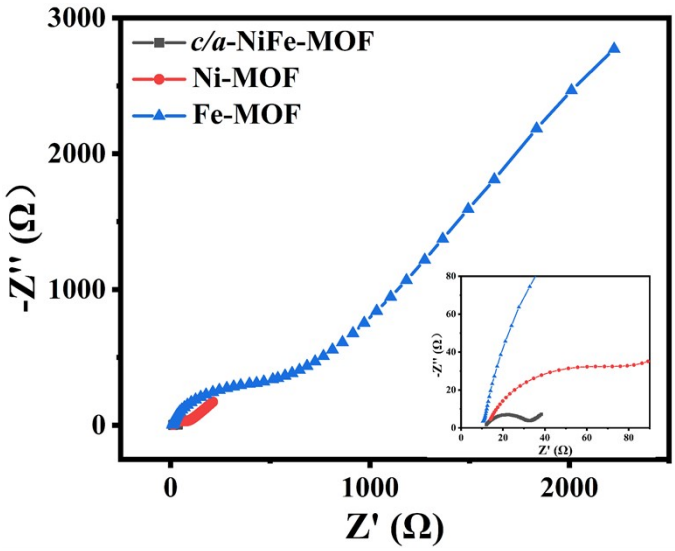


**Fig. S15.** Nyquist plots of *c/a*-NiFe-MOF, Fe-MOF, and Ni-MOF.

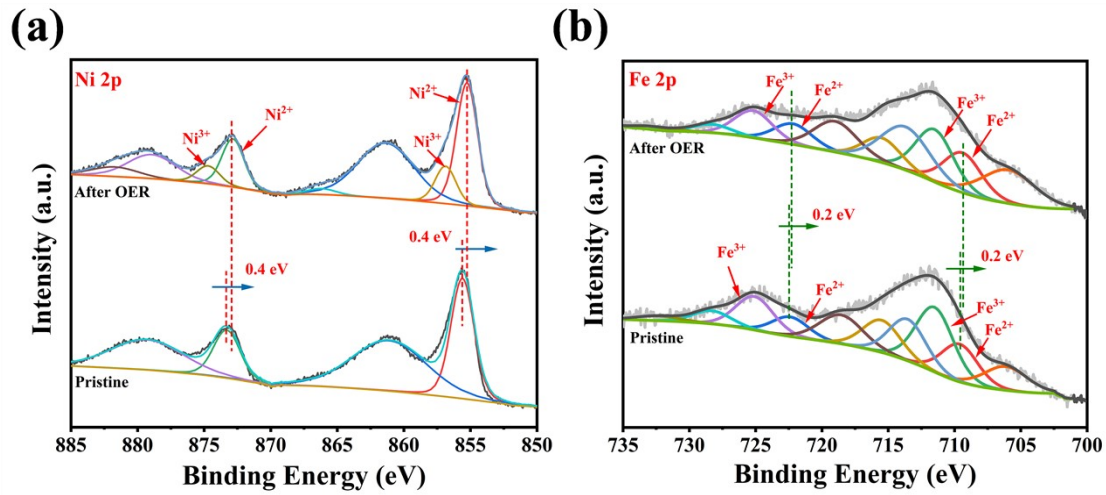


**Fig. S16.** High resolution XPS spectra of Ni 2p region and Fe 2p region after OER test.

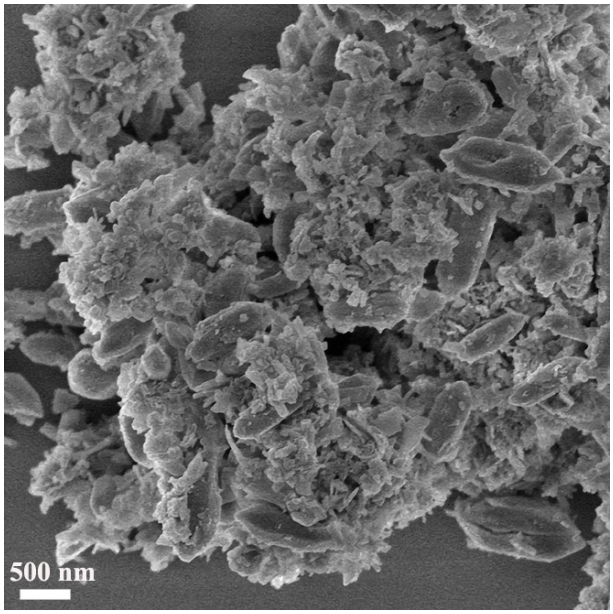


**Fig. S17.** The SEM image of *c/a*-NiFe-MOF after OER test.

The *c/a*-NiFe-MOF after OER test still maintain the structure of heterostructure which comprised of nanoparticles and spindles.

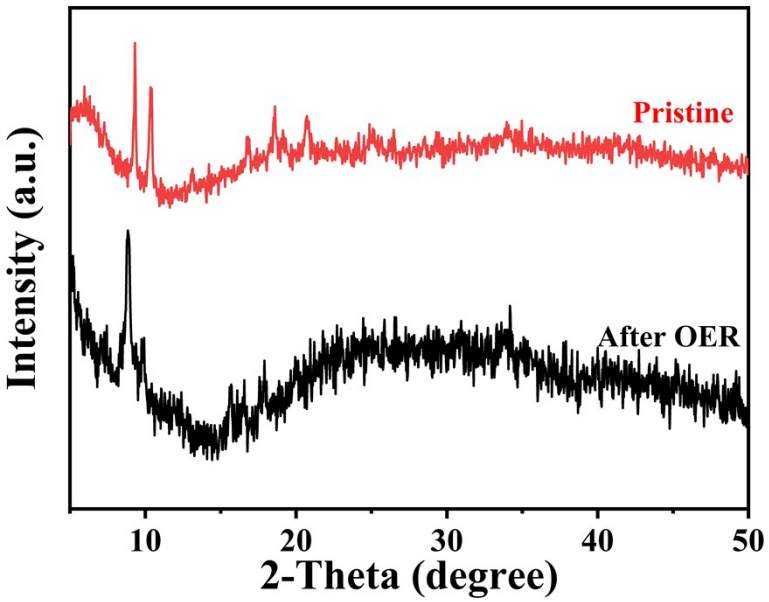


**Fig. S18.** The XRD pattern of *c/a*-NiFe-MOF before and after OER test.

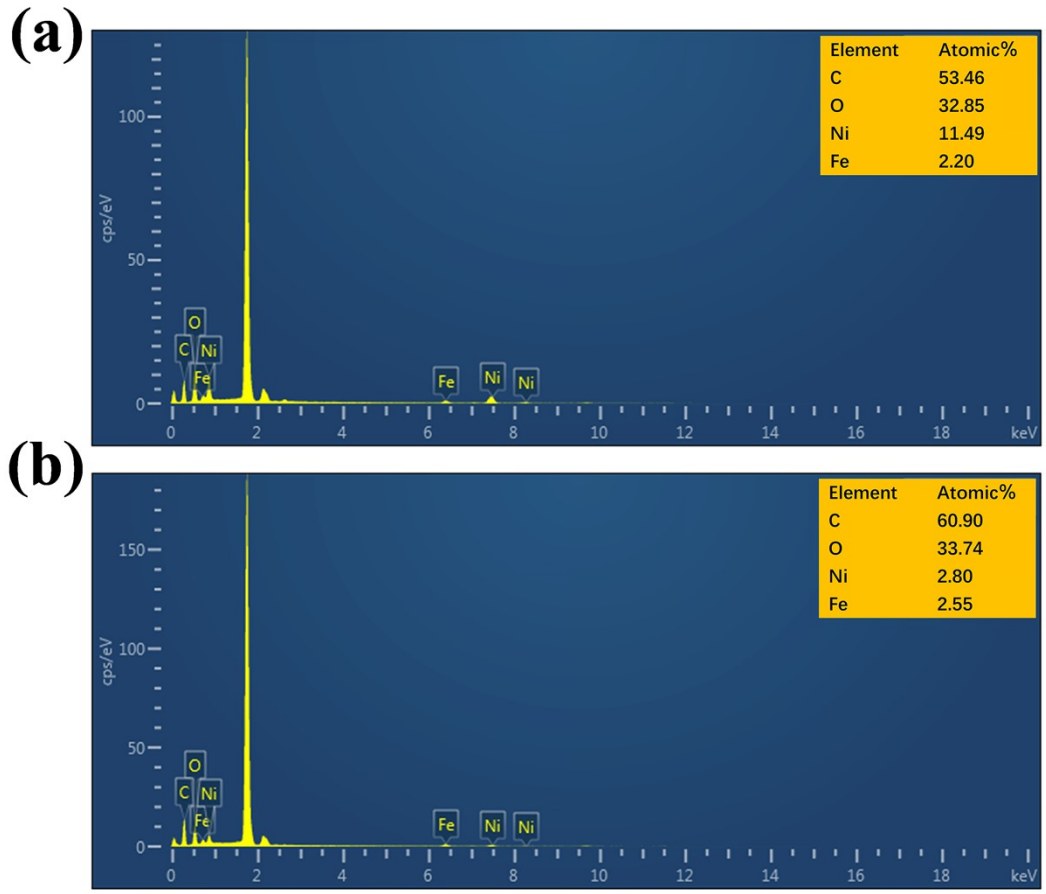


**Fig. S19.** (a) The EDS of nanoparticles in *c/a*-NiFe-MOF after OER test, and (b) the EDS of the spindles in *c/a*-NiFe-MOF after OER test.

The ratio of Ni/Fe was 1.10:1 for spindles and 5.22:1 for nanoparticles after OER test, which is very close to the content of sample before OER (Ni/Fe was 0.92:1 for spindles and 4.82:1 for nanoparticles)

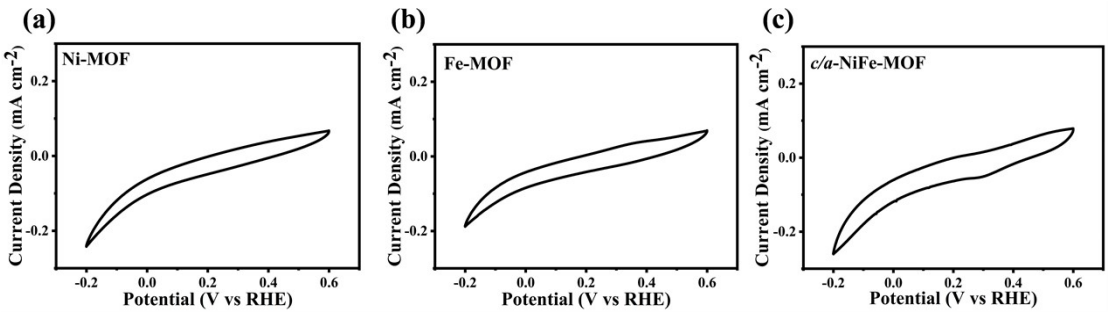


**Fig. S20.** CV curves of (a) Ni-MOF, (b) Fe-MOF, and (c) *c/a*-NiFe-MOF in PBS solution (pH = 7.0) at a scan rate of 50 mV $s^{-1}$.

## Tables

**Table S1.** Comparison of OER activity of *c/a*-NiFe-MOF and Ni/Fe-based electrocatalysts tested in KOH.

| Catalysts | Overpotential (mV) at 10 mA $cm^{-2}$ | Tafel slope/mV $dec^{-1}$ | References |
|---|---|---|---|
| ***c/a*-NiFe-MOF** | **236** | **30** | **This Work** |
| NiFe-UMN | 260 | 30 | **Nano Energy.** 2018**,** 44, 345–352 |
| Fe1Ni2-BDC | 260 | 42 | **ACS Energy Lett**. 2019, 4, 285−292 |
| NiFe-MOF array | 240 | 34 | **Nat. Commun.** 2017, 8, 15341 |
| 2D-MOF Fe/Co (1:2) | 238 | 52 | **Angew. Chem. Int. Ed.** 2021, 60, 12097 – 12102 |
| $(Ni_2Co_1)_{0.925}Fe_{0.075}$-MOF-NF | 257 | 41.3 | **Adv. Mater.** 2019, 31, 1901139 |
| CoFe-MOF | 265 | 44 | **ACS Catal.** 2019, 9, 7356-7364. |
| Co-MOF | 263 | 44 | **J. Mater. Chem. A**. 2018, 6, 22070-22076. |
| Ni-MOF@Fe-MOF | 265 | 82 | **Adv. Funct. Mater.** 2018, 28, 1801554. |
| $Co_3S_4$@$MoS_2$ | 280 | 43 | **Nano Energy** 2018, 47, 494 |
| Co-N-C | 321 | 40 | **J. Am. Chem. Soc.** 2019, 141, 14190-1419. |

**Table S2**. The calculated value of n based on CV results and the value of TOF.

| Sample | n ($10^{-7}$ mmol) based on CV results | TOF ($S^{-1}$) |
|---|---|---|
| *c/a*-NiFe-MOF | 2.32 | 10.2 |
| Fe-MOF | 1.66 | 0.3 |
| Ni-MOF | 1.61 | 3.3 |

**Table S3**. The calculated value of n based on ICP results and the value of TOF.

| Sample | n ($10^{-7}$ mmol) based on ICP results | TOF ($S^{-1}$) |
|---|---|---|
| *c/a*-NiFe-MOF | 68.4 | 0.37 |
| Fe-MOF | 82.8 | 0.016 |
| Ni-MOF | 94.8 | 0.056 |

**Table S4.** The ohmic contact resistances ($R_s$) and charge transfer resistance ($R_{ct}$) are obtained from the equivalent circuit of different samples.

| Sample | $R_s$/Ω | $R_{ct}$/Ω |
|---|---|---|
| *c/a*-NiFe-MOF | 11.1 | 20.7 |
| Ni-MOF | 12.4 | 75.1 |
| Fe-MOF | 10.1 | 602.4 |

1. F. Sun, G. Wang, Y. Ding, C. Wang, B. Yuan and Y. Lin, *Adv. Energy Mater.*, 2018, **8**, 1800584.
2. R. Liang, F. Jing, L. Shen, N. Qin and L. Wu, *J. Hazard. Mater.*, 2015, **287**, 364-372.
3. S. Bordiga, C. Lamberti, G. Ricchiardi, L. Regli, F. Bonino, A. Damin, K. P. Lillerud, M. Bjorgen and A. Zecchina, *Chem. Commun.*, **2004**, 20, 2300-2301.
4. J. Li, W. Huang, M. Wang, S. Xi, J. Meng, K. Zhao, J. Jin, W. Xu, Z. Wang, X. Liu, Q. Chen, L. Xu, X. Liao, Y. Jiang, K. A. Owusu, B. Jiang, C. Chen, D. Fan, L. Zhou and L. Mai, *ACS Energy Lett*., 2018, **4**, 285-292